Aging effect on microcirculation: A multiscale entropy approach on laser speckle contrast images

Adil Khalil, Anne Humeau-Heurtier, L. Gascoin, Pierre Ábrahám, Guillaume Mahé

Aging effect on microcirculation: a multiscale entropy approach on laser speckle contrast images

A. Khalil* and A. Humeau-Heurtier†

University of Angers, LARIS–Laboratoire Angevin de Recherche en Ingénierie des Systèmes, 62 avenue Notre-Dame du Lac, 49000 Angers, France

L. Gascoin

University of Angers, Hospital of Angers, Laboratoire de Physiologie et d'Explorations Vasculaires, 49033 Angers cedex 01, France

P. Abraham

University of Angers, Hospital of Angers, Laboratoire de Physiologie et d'Explorations Vasculaires, UMR CNRS 6214-INSERM 1083, 49033 Angers cedex 01, France

G. Mahé

Pôle imagerie médicale et explorations fonctionnelles, Inserm CIC 1414, Hospital Pontchaillou of Rennes, University of Rennes 1, 35033 Rennes Cedex 9, France

Abstract

Purpose: It has long been known that age plays a crucial role in deterioration of microvessels. The assessment of such deteriorations can be achieved by monitoring microvascular blood flow. Laser speckle contrast imaging (LSCI) is a powerful optical imaging tool that provides two-dimensional information on microvascular blood flow. The technique has recently been commercialized, and hence, few works discuss the postacquisition processing of laser speckle contrast images recorded *in vivo*. By applying entropy-based complexity measures to LSCI time series, we present herein the first attempt to study the effect of aging on microcirculation by measuring the complexity of microvascular signals over multiple time scales.

Methods: Forearm skin microvascular blood flow was studied with LSCI in 18 healthy subjects. The subjects were subdivided into two age groups; younger (20–30 years old, n=9) and older (50–68 years old, n=9). To estimate age-dependent changes in microvascular blood flow, we applied three entropy-based complexity algorithms to LSCI time series.

Results: The application of entropy-based complexity algorithms to LSCI time series can differentiate younger from older groups: the data fluctuations in the younger group have a significantly higher complexity than those obtained from the older group.

Conclusion: The effect of aging on microcirculation can be estimated by using entropy-based complexity algorithms to LSCI time series.

I. INTRODUCTION

It has been reported that age changes the structure of the cutaneous microvasculature[1], and plays a crucial role in cardiovascular diseases[2]. In recent years, optical medical imaging has been the focus of considerable attention for the monitoring of peripheral cardiovascular regulation, mainly microvascular blood flow. Several optical tools have emerged to monitor microvascular blood flow[3–7]. Laser speckle contrast imaging (LSCI) is gaining an increased interest in medical research due to its high performance-to-cost ratio: LSCI is a noninvasive, contactless, and highly reproducible technique[8–10]. Moreover, LSCI provides high quality images of the microvascular blood flow at low cost[11].

The principle behind the LSCI technique is based on a laser beam and a camera (a schematic diagram of a LSCI setup is shown in Fig. 1). When a laser light illuminates the tissue under study, the backscattered photons form a random interference pattern – called speckle pattern – on the camera. The fluctuations in the illuminated tissue (due to the moving particles such as red blood cells) lead to temporal changes in the speckle pattern. These fluctuations provide information about the movements of the scatterers. The exposure time T of the camera causes a blurring of speckle pattern, and hence, leads to a reduction in the local speckle contrast. The speckle contrast K is used to quantify the degree of blurring[12]

$$K(x,y) = \frac{\sigma_N}{\mu_N}, \tag{1}$$

where σ_N and μ_N are the spatial standard deviation and the mean intensity, respectively, in a square around the pixel of coordinates (x, y). In order to quantify σ_N and μ_N, a square window of $N \times N$ pixels is therefore chosen around the pixel $P(x, y)$ of the speckle raw data. The speckle contrast is computed by processing a group of pixels in one image. The contrast is therefore the spatial contrast. However, a temporal contrast computation can also be used by taking multiple images and following the same pixel in a time sequence[13].

To assess the microcirculation function, a critical task is to obtain relevant physiological information from medical images. Thus, many signal and image processing methods have been proposed in order to allow a better understanding of the underlying physiological characteristics. Among these methods, the sample entropy computation has become of great interest in the biomedical field[14]. It has been used to measure the regularity of physiological

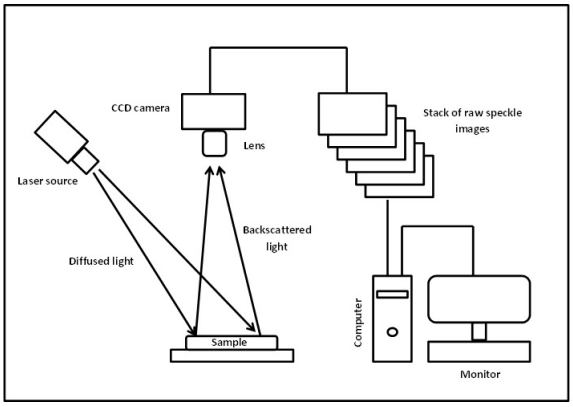

FIG. 1. Schematic diagram of a LSCI setup.

time series[15–17]. However, sample entropy is a single scale analysis, whereas the cardiovascular system manifests in multiple temporal scales to increase its adaptive capacity in an evolving environment. Hence, the complexity of the cardiovascular system operates in multiple temporal scales. Therefore, single scale entropy analyses do not provide multiple level information on the behavior of the complex physiological system. To overcome this drawback, multiscale entropy (MSE, see Sec. II E) has been introduced as a useful tool to process physiological signals in multiple time scales[18,19], relying on the same principles as sample entropy statistics. MSE analyses are widely used on data recorded from the macrocirculation for the diagnosis of different kinds of pathologies, but also to analyze the impact of aging[18,20–22]. The MSE algorithm has also been applied by Humeau-Heurtier *et al.*[23,24] to LSCI data obtained from the microvascular system. In their studies, the efforts were made to better understand the perfusion time series given by LSCI. However, no study related to aging was performed. In addition, in our previous work[25], we analyzed the aging effect over microvascular parameters (perfusion and moving blood cells velocity from LSCI data) and macro-circulation parameters (pulse-wave velocity), and the relationship between these parameters. However, the signal processing tools used in those previous studies are different from the ones proposed in the present work. To the best of our knowledge, the impact of aging on the microcirculation has not been studied yet by using entropy-based complexity algorithms on LSCI data. The latter having good temporal and spatial resolutions, they could be of interest in the follow-up of age-dependent microvascular alterations. Other laser-based studies have been conducted to study the influence of age[26]. Therefore, by processing laser speckle contrast images, the purpose of this study is to determine if alterations of micro-

circulation caused by aging can be studied through complexity measures. For this purpose, MSE and its refined versions, composite MSE (CMSE), and refined CMSE (RCMSE), are applied to LSCI time series. Furthermore, a comparison of the results given by MSE, CMSE, and RCMSE algorithms is proposed. In what follows, we first introduce the measurement procedure and theoretical background. The experimental results are presented in Section III. Then, a discussion is proposed in Section IV. Finally, conclusions are given in Section V.

II. MATERIALS AND METHODS

A. Subjects

Eighteen healthy subjects without known history of disease were included in this study. The subjects were divided into two age groups: younger and older. The younger group included nine subjects (five women and four men), ranging from 20 to 30 years. The older group included nine subjects (five women and four men), ranging from 50 to 68 years. Prior to participation, all subjects gave their written, informed consent, and the study was conducted in accordance with the Declaration of Helsinki.

B. Experimental protocol

For the application of MSE, CMSE, and RCMSE to LSCI time series, all the perfusion images were acquired from the ventral face of the forearm using a PeriCam PSI System (Perimed, Sweden). The imager has a laser wavelength of 785 nm and an exposure time of 6 ms. In this imager, the speckle pattern in the illuminated area is monitored using a 1388×1038 pixels CCD camera (Perimed, Sweden), and the contrast is thereafter computed spatially. Perfusion (computed from the inverse of the contrast K) is then processed in our work.

The laser speckle contrast imaging technique is, by definition, very sensitive to movements. Therefore, the subjects were asked to be supine and avoid moving during the data acquisition. Before processing the LSCI data with the entropy-based measures, no preprocessing was performed to remove the possible presence of outliers (we took care to check that outliers, if present, were very few and of low amplitude, see Fig. 2).

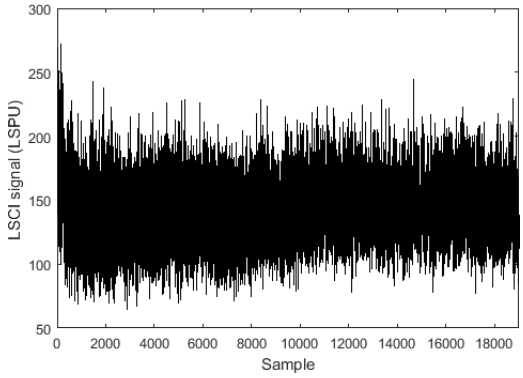

FIG. 2. Relative blood flow time course computed from LSCI data during 20 min at rest. LSCI signal computed from a region of interest of 31×31 pixels.

The superficial blood flow was recorded in laser speckle perfusion units (LSPU) with a sampling frequency of 16 Hz. A temperature-controlled room[27] without any airstream[28] was used for this purpose. Moreover, the distance between the laser head and the forearm skin was adjusted to 15 ± 1 cm[29] which provided images with a resolution of around 0.45 mm. Perfusion images were stored on a computer for an off-line analysis.

In this work, 19000 images (around 20 minutes) for each subject were processed. This length has been chosen to have access to low frequency oscillations already found in other microvascular data[30–32].

C. Image processing procedure

In order to analyze complexity of LSCI time series, the following image processing steps were used:

1. On the first perfusion image of each subject, one pixel was chosen arbitrarily, and its perfusion was followed in time for all the 19000 successive perfusion images

2. To get a reasonable signal and reduce the spatial variability of blood flow[33], an average perfusion value was computed inside a region of interest (ROI) around each of the pixels chosen in step 1 and followed with time. This resulted in a new time evolution signal. For this purpose, ROI of different sizes were analyzed as suggested by[23]: 1×1 pixel, 3×3 pixels, 9×9 pixels, 15×15 pixels, 23×23 pixels, and 31×31 pixels. A previous

work[23] has reported that MSE values for ROI sizes larger than 23×23 pixels are close to the ones obtained with an ROI of size 23×23 pixels. This is why the largest ROI size chosen in our work was not larger than 31×31 pixels

3. For each ROI size (1×1, 3×3, 9×9, 15×15, 23×23, and 31×31 pixels), MSE, CMSE, RCMSE values were estimated and presented as a function of scale factor, τ

D. Statistical analysis

Because of the small size of the sample (only 9 subjects in each group), the normality of the distribution for each variable (ROI 1×1 pixel; ROI 3×3 pixels; ROI 9×9 pixels; ROI 15×15 pixels; ROI 23×23 pixels and ROI 31×31 pixels) was checked using Shapiro-Wilk test. The results showed normal distribution for both younger and older groups, and for all ROI sizes. Therefore, statistical analyses were performed using a t-test analysis (unpaired, two-tailed) to compare ROI of the young group with ROI of the old group after checking for the equality of variances (F-test). Thus, for the two populations (young subjects and old subjects) we computed the sum of RCMSE values over the scales studied (106 to 1684; see below), and this for all the ROI sizes studied: 1×1 pixel, 3×3 pixels, 9×9 pixels, 15×15 pixels, 23×23 pixels, and 31×31 pixels. This gave an index for the two populations, and for each ROI size. We performed a statistical analysis on this index to compare the results between the young subjects and the older ones, for each ROI size. For all statistical analyses, a two-tailed p value < 0.05 was considered significant.

E. Methods

1. Multiscale entropy

The MSE approach aims at evaluating the underlying complexity of the dynamic system across multiple time scales. In this study, MSE was computed as initially introduced[19]. For a given one-dimensional vector of data, $\{x_1, ..., x_i, ...x_N\}$, groups of successive points are time-binned to create a coarse-grained time series, $\{y^{(\tau)}\}$. For this purpose, the original times series are subdivided into nonoverlapping groups of length τ. Then, an average of the data points inside each group is performed. The steps mentioned above to generate a

coarse-grained time series are accomplished using the equation

$$y_j^{(\tau)} = \frac{1}{\tau} \sum_{i=(j-1)\tau+1}^{j\tau} x_i, \qquad 1 \leq j \leq N/\tau. \tag{2}$$

Finally, each coarse-grained time series is evaluated by computing an entropy measure (sample entropy, SampEn)[14]. The result is displayed versus the scale factor, τ.

The SampEn algorithm is a conditional probability concept that two embedded subsets that are close to each other for m successive points, within a given tolerance r, will also remain close to each other if one more point is embedded to each subset. For data of N samples, $N-m$ vectors $x_m(i)$ are constructed for $\{i|1 \leq i \leq N-m\}$ as $x_m(i) = \{x(i+k) : 0 \leq k \leq m-1\}$. The distance d between two vectors $x_m(i)$ and $x_m(j)$ is defined as $d\left[x_m(i), x_m(j)\right] = max\{|x(i+k) - x(j+k)| : 0 \leq k \leq m-1\}$. Then, $B_i^m(r)$ is computed as $(N-m-1)^{-1}$ times the number of vectors $x_m(j)$ within r of $x_m(i)$ where j ranges from 1 to $N-m$ and $j \neq i$ (self-matches are excluded). $B^m(r)$ is thus determined as

$$B^m(r) = (N-m)^{-1} \sum_{i=1}^{N-m} B_i^m(r), \tag{3}$$

where

$$B_i^m(r) = \frac{n_i^m(r)}{(N-m-1)}, \tag{4}$$

$B^m(r)$ is the probability that two sequences will match for m points, and n_i^m represents the number of vectors $x_m(j)$, such that $d\left[x_m(i), x_m(j)\right] \leq r$. $B^{m+1}(r)$ is the probability that two sequences will match for $m+1$ points, and is computed in the same way as in Eq. 3. The sample entropy ($SampEn(m,r)$) is then defined as

$$SampEn(m,r) = \lim_{N \to +\infty} \left\{ -\ln \left[\frac{B^{m+1}(r)}{B^m(r)} \right] \right\}. \tag{5}$$

For finite N, it is estimated by the statistics as[14]

$$SampEn(m,r,N) = -\ln \left[\frac{B^{m+1}(r)}{B^m(r)} \right]. \tag{6}$$

The SampEn algorithm has proved to be useful for relatively short and noisy datasets[14].

Thus, for each constructed coarse-grained time series mentioned in Eq. 2,

$$MSE(x, \tau, m, r) = -\ln\left(\frac{n_\tau^{m+1}}{n_\tau^m}\right), \tag{7}$$

where n_τ^m represents the total number of m-dimensional matched vector pairs and is constructed from the coarse-grained time series at a scale factor of τ.

In the MSE algorithm, estimated values of SampEn are plotted *versus* the scale factors, τ. These entropy values are used for assessing the complexity degree of normalized time series. An increasing or consistent behavior of the entropy values *versus* an increase in scale factors indicates that the original time series is highly complex, containing information over multiple time scales. In contrast, a decrease in entropy values with scale factors shows that the original time series carries information only on the smallest scales.

Two important parameters have to be considered during the estimation of SampEn values: the tolerance degree r, and the pattern length m. Previous studies have shown that $m = 1$ or 2, and $r = [0.1, 0.25]$ of the standard deviation of the original signal are adequate to obtain good statistical validity for SampEn[14]. As used previously for microvascular data studies[34,35], $m = 2$, and $r = 0.15 \times$ standard deviation of the signal were chosen herein. Furthermore, in order to reveal microvascular physiological activities, acting in a time scale interval τT of 6.625–105.25 s[30–32], a wide range of scale factors was analyzed: scale factors τ ranging from 106 to 1684.

2. Composite multiscale entropy

CMSE was introduced to reduce the variance of estimated entropy values of MSE at large scale factors τ[36]. Unlike MSE, CMSE generates k-child coarse-grained time series for each scale factor τ. So, for a given discrete time series $\{x_1, ..., x_i, ...x_N\}$, the kth-child coarse-grained time series for scale factor τ is produced as[36] $y_k^{(\tau)} = \{y_{k,1}^{(\tau)}\ y_{k,2}^{(\tau)}...y_{k,p}^{(\tau)}\}$ where

$$y_{k,j}^{(\tau)} = \frac{1}{\tau}\sum_{i=(j-1)\tau+k}^{j\tau+k-1} x_i, \qquad 1 \le j \le N/\tau, 1 \le k \le \tau. \tag{8}$$

Then, for each scale factor τ, sample entropy values are estimated for all k-child coarse-grained groups. The mean value of the τ entropy values corresponds to CMSE[36].

$$CMSE(x,\tau,m,r) = \frac{1}{\tau}\sum_{k=1}^{\tau}\left(-\ln\frac{n_{k,\tau}^{m+1}}{n_{k,\tau}^{m}}\right), \tag{9}$$

where $n_{k,\tau}^{m}$ is the total number of m-dimensional matched vector pairs and is computed from the kth-child coarse-grained time series at a scale factor τ. Different from MSE, the CMSE algorithm provides higher entropy reliability on both synthetic and real data[36].

3. Refined composite multiscale entropy

Although CMSE provides higher reliability in entropy estimation than traditional MSE, the probability that CMSE fails to produce an estimate of the entropy becomes higher when the complexity measure is applied to short time series. To overcome this drawback, RCMSE was proposed[37]. From Eq. (9), we can observe that when CMSE is computed, undefined entropy is obtained when either $n_{k,\tau}^{m+1}$ or $n_{k,\tau}^{m}$ is zero. Thus, the shorter the time series, the more the probability of having an undefined entropy. Consequently, CMSE has better accuracy estimation than traditional MSE, but at the expense of entropy estimation ability. Therefore, RCMSE addressed this drawback based on the following equation[37]

$$RCMSE(x,\tau,m,r) = -\ln\left(\frac{\sum_{k=1}^{\tau} n_{k,\tau}^{m+1}}{\sum_{k=1}^{\tau} n_{k,\tau}^{m}}\right). \tag{10}$$

From Eq. (10), it is obvious that RCMSE gives rise to undefined entropy only when all $n_{k,\tau}^{m+1}$ or $n_{k,\tau}^{m}$ are zero. Accordingly, RCMSE increases the ability to estimate entropy values compared to CMSE. RCMSE shows reduced variability and data-length dependence than either the MSE or CMSE algorithms when applied to white and and $1/f$ noises[37].

III. RESULTS

In Fig. 3(a) we present the mean experimental results for MSE, CMSE, and RCMSE, for the two groups of subjects, when the value of a LSCI single pixel time series is analyzed. From this figure we can observe that the entropy values obtained from the younger group (blue) and from the aged group (red) are close to each other for all time scales (binning time interval $\tau T = [6.6\text{–}105.2]\,\mathrm{s}$). This is true for MSE, CMSE, and RCMSE. Furthermore, a monotonic decrease in entropy values versus time scale is observed for the two groups.

The reduction in entropy values at large time scales, τT, shows that the analyzed signal is an independent random variable, containing information only at the smallest time scales. This behavior is close to the one of a Gaussian white noise realization[19]. For the analysis of Gaussian white noise data, as the length of the windows used to build coarse-graining time series signal increases, the average value inside each window converges to a fixed value, because no new pattern arises on large scales. Hence, the standard deviation dramatically diminishes with scale factor. The same is found for MSE, CMSE, and RCMSE of LSCI single pixel time series. This reflects that the LSCI single pixel time series have information only at the shortest scales. However, it is worth mentioning that the application of MSE to LSCI data shows small and rapid variations in entropy values when time scales large enough are analyzed. This behavior can be observed when either single pixel or ROI are analyzed (see Figs. 3(a) to 3(f)). In contrast, CMSE and RCMSE manifest a relatively stable decrease during the increase of time scales.

A markedly loss of complexity is observed with aging when a ROI large enough is chosen (see Fig. 3(f)). The difference is hardly visible with a ROI size of 3×3 pixels (see Fig. 3(b)) and increases when ROI size increases (see Fig. 3(f)). There were no significant differences between the younger and older groups on the entropy index values obtained from RCMSE of LSCI single pixel and 3×3 pixels ($p = 0.649$, and $p = 0.259$, respectively). In contrast, the entropy index values of RCMSE LSCI 9×9 pixels, 15×15 pixels, 23×23 pixels, and 31×31 pixels for the younger group are significantly different from the ones obtained from older group ($p = 0.02, p = 0.008, p = 0.007$, and $p = 0.008$, respectively).

From Fig. 3(a), we observe that when MSE and CMSE are applied to experimental LSCI single pixel time series, the probability of undefined entropy was zero. This was not the case after a spatial averaging over neighboring pixels (see Figs. 3(b) to 3(f)). It is obvious from these figures that the validity of both MSE and CMSE is worse when larger scale factors are used. Therefore, the probability that the entropy estimate will be undefined increases as the scale factor increases. It has been shown that the probability that the estimate of MSE and CMSE is undefined increases as the entropy of the time series increases[37]. In MSE, when large scale factors are used to build the coarse-grained time series, the variance increases very fast that may lead to underestimation of entropy (i.e., spike increases observed in

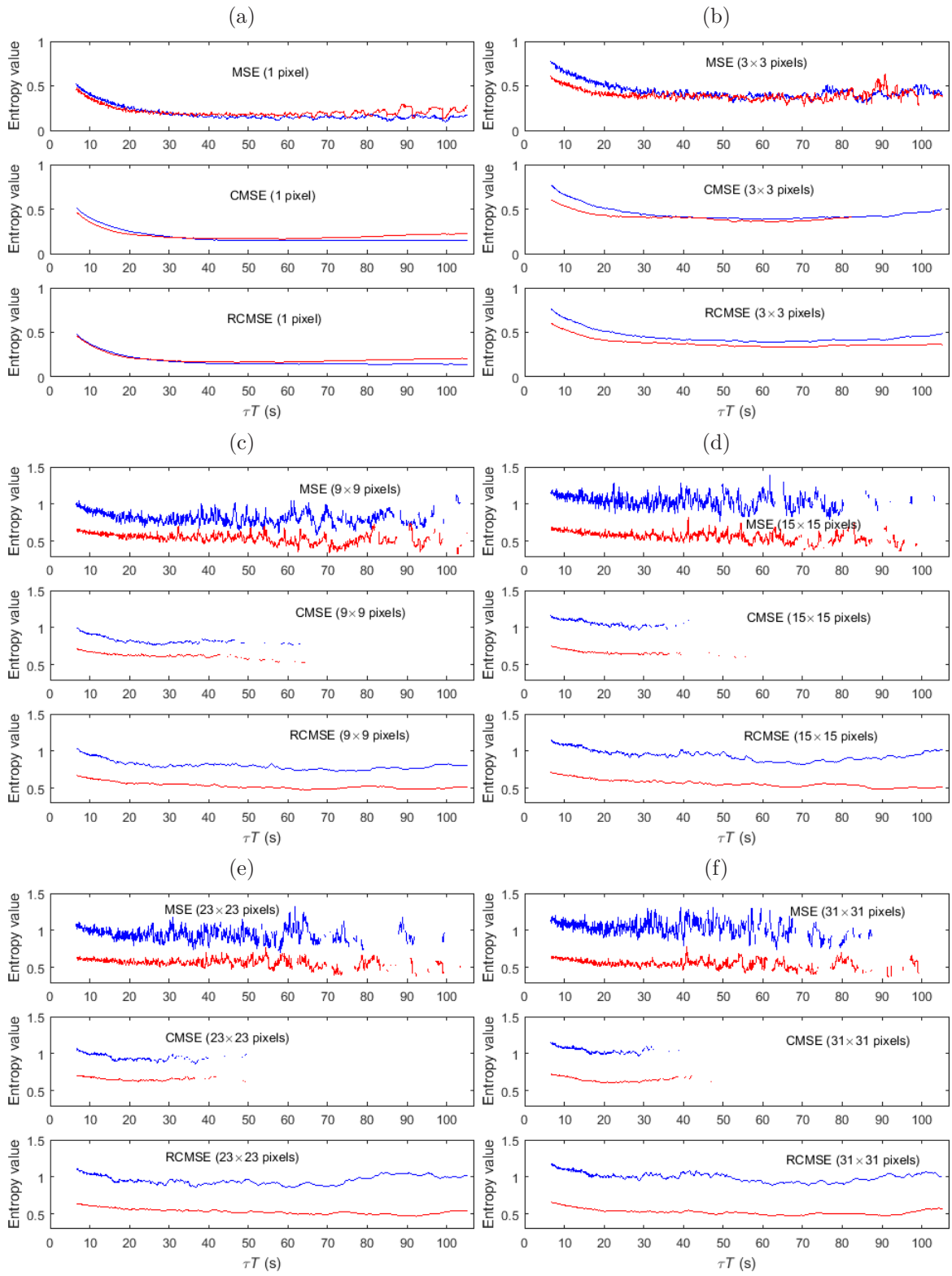

FIG. 3. Mean experimental entropy values for the two healthy groups of subjects: younger group (blue) and older group (red) with 9 subjects in each group. For each subfigure, three methods are shown: MSE (top), CMSE (middle), and RCMSE (bottom). Results for LSCI times series are obtained from (a): 1×1 pixel; (b): 3×3 pixels; (c): 9×9 pixels; (d): 15×15 pixels; (e): 23×23 pixels; (f): 31×31 pixels. A scale factor interval from $\tau = 106$ to $\tau = 1684$ is analyzed, which provides a binning time interval from $\tau T = 6.625\,\mathrm{s}$ to $\tau T = 105.25\,\mathrm{s}$.

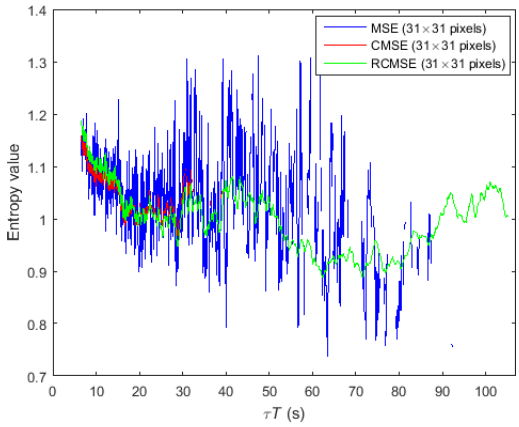

FIG. 4. MSE, CMSE, and RCMSE of LSCI 31×31 pixels time series recorded on healthy subjects. Results are the mean entropy values of 9 younger subjects. A scale factor interval from $\tau = 106$ to $\tau = 1684$ is analyzed, which provides a binning time interval from $\tau T = 6.625\,\mathrm{s}$ to $\tau T = 105.25\,\mathrm{s}$.

entropy values over all the patterns of the MSE), or even undefined entropy values—no template vectors are matched to one another. In contrast, CMSE reduces the variance. This leads to more accurate estimation of entropy values[36]. As it is obvious from Figs. 3(b) to 3(f), CMSE gradually provides higher entropy reliability, and better separability between younger and older groups than MSE. However, CMSE increases the probability of undefined entropy due to the reasons mentioned in Sec. II E, in particular for large time scales[37]. By opposition, and as shown in Fig. 4, RCMSE shows better validity than MSE and CMSE. Therefore, in what follows, RCMSE will be used to present the remaining findings due to its better validity compared to MSE and CMSE.

Within the range of time scales analyzed, one can hypothesize that the strong rhythmic behavior of the peripheral cardiovascular activities may lead to low entropy values. Therefore, peripheral cardiovascular activities could be identified according to their regularities and time-related values. In this respect, we can distinguish two physiologically-linked areas over the pattern of RCMSE, extending between 6.625 s and 105.25 s for the younger subjects (see Fig. 5). First, the entropy values reach a local minimum for binning time interval τT around 31–42 s. The temporal fluctuations around this interval are considered as the first area that has high regularity. The second physiologically-related area is observed around binning time interval of 60–80 s. From Fig. 5 we observe that for the younger group,

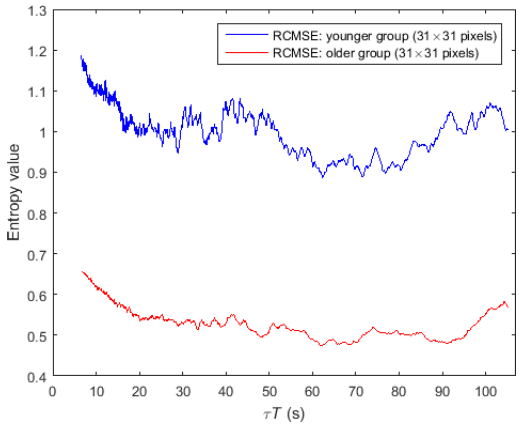

FIG. 5. RCMSE of LSCI 31 × 31 pixels time series recorded on healthy subjects. Results are the mean entropy values of two groups; younger group (blue) and older group (red) of 9 subjects each. A scale factor interval from $\tau = 106$ to $\tau = 1684$ is analyzed, which provides a binning time interval from $\tau T = 6.625\,\mathrm{s}$ to $\tau T = 105.25\,\mathrm{s}$. This is an enlarged version of the RCMSE plot in Fig. 3(f).

the processes acting around this interval of 60–80 s have a high regularity. In contrast, the physiologically-linked areas over the pattern of RCMSE for older group have weaker features. From Fig. 5, the first local minimum for the older group can be observed around 48 s, whereas a second global area is between 60–70 s, and another close to 90 s.

IV. DISCUSSION

From Figs. 3(a) to 3(f), we have observed that the application of MSE to LSCI data shows small and rapid variations in entropy values when time scales large enough are analyzed. The same behavior of small and rapid variations in entropy values at large scale factors has been observed by the application of MSE to successive signals of a pulse wave velocity[38]. In MSE, the variance increases as large scale factors are used to build the coarse-grained time series, that may lead to underestimation of entropy. Furthermore, from Figs. 3(b) to 3(f), we observe that choosing larger ROI sizes modifies the behavior of MSE, CMSE, and RCMSE. The modifications of MSE, CMSE, and RCMSE trends with ROI show that LSCI ROIs do not behave as Gaussian white noise. The signal-to-noise ratio increases as the ROI increases[23].

We have mentioned above from Figs. 3(b) to 3(f) that the validity of both MSE and CMSE is worse when large scale factors are used. This experimental finding is in agreement with the theoretical study of Wu *et al.*[37], where correlated and uncorrelated noises were analyzed. They found that the validity degree of the MSE and CMSE depends on the time series length, and entropy values of the time series: the larger the scale factors, the shorter the coarse-grained time series. Our signals contain 19000 data points, and therefore, the shortest coarse-grained time series contain 11 points. As a result to all mentioned above, MSE, CMSE, and RCMSE are able to estimate the underlying complexity of LSCI signals. However, RCMSE provides better validity for short time series.

We demonstrate that the application of MSE, CMSE, and RCMSE to microvascular data (LSCI time series) can remarkably differentiate between younger and older groups: the fluctuations of the younger group show higher complexity than those obtained from the older group. The loss of complexity within the microvascular blood flow signal may be explained as a consequence of changes occurring within the cardiovascular system. We have previously mentioned that macro- and microcirculation are correlated systems[25]. It has been reported that the cardiac fluctuations of healthy young subjects are highly complex, but this complexity decreases with aging[39–42].

A living organism system is a highly complex system. This complexity comes from a wide range of adaptive reactions to different physiological variables within the external environment. Therefore, physiological complexity of the living system reflects its ability to adapt to the ever-changing circumstances, that will be needed to merge multiscale processes. Alternatively, under baseline condition, a continuous decrease in complexity reflects damaged physiological responses of the living organism to changes in the external environment[18]. By the application of MSE to macrovascular data, a loss of the complexity in cardiac signal has been observed due to aging[18]. A reduction in signal complexity with aging has also been reported when nonlinear measures are applied to successive signals of a pulse wave velocity[43]. Furthermore, it has been shown that aging has a crucial role on the interconnection network of the cardiovascular system[44,45]. For example, several modifications in cardiac electrophysiology, including an increase in sympathetic nervous system activity[46], or alterations in the muscular tissue of the heart, appear with aging[47]. Wu *et al.*[48] demonstrated a reduction

of complexity with age of both the heart and blood vessels signals. Diminished functional responses to stimuli have been reported by many authors as a distinctive attribute of age-related pathology[49–51]. Other authors have recently mentioned that the relation between QT and RR interval variability derived from the heart deteriorates with aging[52]. Our first finding confirms a general complexity loss with aging on LSCI data (microvascular blood flow). Furthermore, we demonstrate that the entropy-based complexity measures when applied to microvascular signal (LSCI time series) can differentiate between younger and older groups.

Alterations in microvascular activities with aging have been reported in many previous studies[53,54]. A reduction in the amount of oxygen reaching the tissues, and unbalance in constructive and destructive metabolism processes may occur with aging[55–57]. Furthermore, a reduction in functioning capillary numbers, and a defect in their basic functions may appear with aging due to phenomena such as vascular rarefaction, regularity loss, vascular destruction, irregular calibration, and attenuation of angiogenesis processes[53,58–61]. It has been pointed out that vascular destruction and oxidant stress contribute to capillary rarefaction[62]. Aging is associated with inhibition of endothelial function and cellular chemical processes, deterioration of the sympathetic innervation[63,64]. Moreover, aging leads to a deterioration in nitric oxide, prostanoid, endothelium derived hyperpolarizing factor(s) and endothelin-1 pathways[62]. It has also been shown that collagen and elastic fibers are damaged with aging[65,66]. Furthermore, one might hypothesize that the reduced complexity of the older group may be connected with age-related structural changes in the skin. It has been reported that a number of physiological features vary with age, including collagen structure, water accumulation, and the thickness of the epidermis, dermis, and the skin as a whole (see Ref.[67] for review).

It is worth mentioning that, from Fig. 5, the profiles of RCMSE of the younger group are slightly different from the ones of the older group. These differences could be due to the following reasons: 1) the movement artifacts. LSCI is highly sensitive to movements. Therefore, it is difficult to have long acquisitions without any movement artifacts. However, it has been shown that a signal contaminated by a small percentage of outliers may remarkably change the standard deviation but not substantially alter the temporal structure of

the time series[18]. Another algorithm dedicated to signals with outliers could also be used to process LSCI data[68]; 2) the average entropy values computed from the seven subjects. Each microvascular activity does not fluctuate at exactly the same period time for each subject. These fluctuations may lead to different patterns in entropy values.

Finally, in the present contribution, we identified two physiologically-linked areas according to their regularities and time-related values. The first area is related to binning time interval between 31 s and 42 s for younger group, and around 48 s for older group. It has been shown that the neurogenic activities are linked to this time interval of 31–48 s[69,70]. The second area that has a high regularity is observed around the binning time interval of 60–80 s for younger group, and around 60–70 s, and another close to 90 s for the older group. The interval between 60–90 s has been previously observed in blood flow signals using time-frequency analyses[30], and as well as in HRV signals[31]. The periodic process around this interval is considered as a marker of endothelial activity[30].

V. CONCLUSION

To the best of our knowledge, this study is considered as the first one conducted to analyze the effect of aging on microcirculation of healthy subjects by applying entropy-based complexity measures to LSCI time series. The MSE, CMSE, and RCMSE algorithms are able to differentiate the younger group from the older group. RCMSE is a simple method for evaluating the complexity of the physiological signal through short time series. It could be interesting now to conduct a similar study on data recorded from another body site (such as the leg or the contra-lateral forearm). Furthermore, it may be of utility in the clinical research to analyze RCMSE values of LSCI data recorded in pathological subjects.

ACKNOWLEDGMENTS

We gratefully acknowledge the support provided by the ministry of higher education and scientific research in Iraq (Baghdad), the Embassy of France in Iraq (service of cooperation and cultural action in Baghdad), and Campus France Paris, France.

The authors declare no conflict of interest.

---

* adil.khalil@etud.univ-angers.fr

† anne.humeau@univ-angers.fr Tel.: +33.(0)2.44.68.75.87

[1] L. Li, S. Mac-Mary, J. M. Sainthillier, S. Nouveau, O. de Lacharriere, and P. Humbert, "Age-related changes of the cutaneous microcirculation in vivo," Gerontology 52, 142–153 (2006).

[2] S. S. Najjar, A. Scuteri, and E. G. Lakatta, "Arterial aging: is it an immutable cardiovascular risk factor?," Hypertension 46, 454–462 (2005).

[3] R. Bi, J. Dong, C. L. Poh, and K. Lee, "Optical methods for blood perfusion measurement–theoretical comparison among four different modalities," J. Opt. Soc. Am. 32, 860–866 (2015).

[4] J. Allen and K. Howell, "Microvascular imaging: techniques and opportunities for clinical physiological measurements," Physiol. Meas. 35, R91–R141 (2014).

[5] S. Eriksson, J. Nilsson, and C. Sturesson, "Non-invasive imaging of microcirculation: a technology review," Med. Device Diagn. Ind. 7, 445–452 (2014).

[6] A. Humeau-Heurtier, E. Guerreschi, P. Abraham, and G. Mahe, "Relevance of laser Doppler and laser speckle techniques for assessing vascular function: state of the art and future trends," IEEE Trans. Biomed. Eng. 60, 659–666 (2013).

[7] C. Huang, D. Irwin, Y. Lin, Y. Shang, L. He, W. Kong, W. Kong, J. Luo, and G. Yu, "Speckle contrast diffuse correlation tomography of complex turbid medium flow," Med. Phys. 42, 4000–4006 (2015).

[8] A. Humeau-Heurtier, P. Abraham, S. Durand, and G. Mahé, "Excellent inter-and intra-observer reproducibility of microvascular tests using laser speckle contrast imaging," Clin. Hemorheol. Microcirc. 58, 439–446 (2014).

[9] C. Puissant, P. Abraham, S. Durand, A. Humeau-Heurtier, S. Faure, et al., "Reproducibility of non-invasive assessment of skin endothelial function using laser Doppler flowmetry and laser speckle contrast imaging," PloS One 8, e61320 (2013).

[10] M. Roustit, C. Millet, S. Blaise, B. Dufournet, and J. L. Cracowski, "Excellent reproducibility of laser speckle contrast imaging to assess skin microvascular reactivity," Microvasc. Res. 80, 505–511 (2010).

[11] L. M. Richards, S. M. Shams Kazmi, J. L. Davis, K. E. Olin, and A. K. Dunn, "Low-cost laser

speckle contrast imaging of blood flow using a webcam," Biomed. Opt. Express 4, 2269–2283 (2013).

[12] J. D. Briers and S. Webster, "Laser speckle contrast analysis (LASCA): a nonscanning, full-field technique for monitoring capillary," J. Biomed. Opt. 1, 174–179 (1996).

[13] P. Li, S. Ni, L. Zhang, S. Zeng, and Q. Luo, "Imaging cerebral blood flow through the intact rat skull with temporal laser speckle imaging," Opt. Lett. 31, 1824–1826 (2006).

[14] J. S. Richman and J. R. Moorman, "Physiological time-series analysis using approximate entropy and sample entropy," Am. J. Physiol. 278, H2039–H2049 (2000).

[15] W. Chen, J. Zhuang, W. Yu, and Z. Wang, "Measuring complexity using fuzzyen, apen, and sampen," Med. Eng. Phys. 31, 61–68 (2009).

[16] A. Humeau, F. Chapeau-Blondeau, D. Rousseau, P. Rousseau, W. Trzepizur, and P. Abraham, "Multifractality, sample entropy, and wavelet analyses for age-related changes in the peripheral cardiovascular system: preliminary results," Med. Phys. 35, 717–723 (2008).

[17] R. Hornero, P. Espino, J. Poza, et al., "Entropy analysis of the EEG background activity in Alzheimer's disease patients," Physiol. Meas. 27, 241 (2006).

[18] M. Costa, A. L. Goldberger, and C. K. Peng, "Multiscale entropy analysis of biological signals," Phys. Rev. E 71, 021906 (2005).

[19] M. Costa, A. L. Goldberger, and C. K. Peng, "Multiscale entropy analysis of complex physiologic time series," Phys. Rev. Lett. 89, 068102–1–068102–4 (2002).

[20] Z. Trunkvalterova, M. Javorka, I. Tonhajzerova, J. Javorkova, Z. Lazarova, K. Javorka, and M. Baumert, "Reduced short-term complexity of heart rate and blood pressure dynamics in patients with diabetes mellitus type 1: multiscale entropy analysis," Physiol. Meas. 29, 817 (2008).

[21] J. Escudero, D. Abásolo, R. Hornero, P. Espino, and M. López, "Analysis of electroencephalograms in Alzheimer's disease patients with multiscale entropy," Physiol. Meas. 27, 1091 (2006).

[22] M. Costa, and I. Ghiran, and C. K. Peng, and A. Nicholson-Weller, and A. L. Goldberger, "Complex dynamics of human red blood cell flickering: alterations with in vivo aging," Phys. Rev. E 78, 020901 (2008).

[23] A. Humeau-Heurtier, G. Mahe, S. Durand, and P. Abraham, "Multiscale entropy study of medical laser speckle contrast images," IEEE Trans. Biomed. Eng. 60, 872–879 (2013).

[24] A. Humeau-Heurtier, M. Baumert, M. Guillaume, A. Pierre, "Multiscale compression entropy

of microvascular blood flow signals: comparison of results from laser speckle contrast and laser Doppler flowmetry data in healthy subjects," Entropy 16, 5777–5795 (2014).

[25] A. Khalil, A. Humeau-Heurtier, G. Mahé, and P. Abraham, "Laser speckle contrast imaging: age-related changes in microvascular blood flow and correlation with pulse-wave velocity in healthy subjects," J. Biomed. Opt. 20, 051010–051010 (2015).

[26] J. A. Knight, K. M. Blackmore, J. Wong, S. Tharmalingam, and L. Lilge, "Optical spectroscopy of the breast in premenopausal women reveals tissue variation with changes in age and parity," Med. Phys. 37, 419-426 (2010).

[27] P. Abraham, M. Bourgeau, M. Camo, A. Humeau-Heurtier, P. Rousseau S. Durand, and G. Mahe, "Effect of skin temperature on skin endothelial function assessment," Microvasc. Res. 88, 56–60 (2013).

[28] G. Mahe, S. Durand, A. Humeau, G. Leftheriotis, P. Rousseau, and P. Abraham, "Air movements interfere with laser speckle contrast imaging recordings," Lasers Med. Sci. 27, 1073–1076 (2011).

[29] G. Mahe, F. Haj-Yassin, P. Rousseau, A. Humeau, S. Durand, G. Leftheriotis, and P. Abraham, "Distance between laser head and skin does not influence skin blood flow values recorded by laser speckle imaging," Microvasc. Res. 82, 439–442 (2011).

[30] A. Stefanovska, M. Bračič, and H. D. Kvernmo, "Wavelet analysis of oscillations in the peripheral blood circulation measured by laser Doppler technique," IEEE Trans. Biomed. Eng. 46, 1230–1239 (1999).

[31] M. Bracic and A. Stefanovska, "Wavelet analysis in studying the dynamics of blood circulation," Nonl. Phen. Compl. Sys. 2, 68–77 (1999).

[32] P. Kvandal, S. A. Landsverk, A. Bernjak, A. Stefanovska, H. D. Kvernmo, and K. A. Kirkebøen, "Low-frequency oscillations of the laser Doppler perfusion signal in human skin," Microvasc. Res. 72, 120–127 (2006).

[33] P. Rousseau, G. Mahé, F. Haj-Yassin, S. Durand, A. Humeau, G. Leftheriotis, and P. Abraham, "Increasing the "region of interest" and "time of interest", both reduce the variability of blood flow measurements using laser speckle contrast imaging," Microvas. Res. 82, 88–91 (2011).

[34] A. Humeau, G. Mahé, F. Chapeau-Blondeau, D. Rousseau, and P. Abraham, "Multiscale analysis of microvascular blood flow: a multiscale entropy study of laser Doppler flowmetry time series," IEEE Trans. Biomed. Eng. 58, 2970–2973 (2011).

[35] A. Humeau, B. Buard, G. Mahé, D. Rousseau, F. Chapeau-Blondeau, and P. Abraham, "Multiscale entropy of laser Doppler flowmetry signals in healthy human subjects," Med. Phys. 37, 6142–6146 (2010).

[36] S. D. Wu, C. W. Wu, S. G. Lin, C. C. Wang, and K. Y. Lee. "Time series analysis using composite multiscale entropy," Entropy 15, 1069–1084 (2013).

[37] S. D. Wu, C. W. Wu, S. G. Lin, K. Y. Lee, and C. K. Peng, "Analysis of complex time series using refined composite multiscale entropy," Phys. Lett. A 378, 1369–1374 (2014).

[38] Y. Chang, H. T. Wu, H. R. Chen, A. Liu, J. Yeh, M. Lo, et al., "Application of a modified entropy computational method in assessing the complexity of pulse wave velocity signals in healthy and diabetic subjects," Entropy 16, 4032–4043 (2014).

[39] P. Lin, M. Lo, J. Tsao, Y. Chang, C. Lin, and Y. Ho, "Correlations between the signal complexity of cerebral and cardiac electrical activity: A multiscale entropy analysis," PLoS One 9, 87798 (2014).

[40] F. Beckers, B. Verheyden, and A. E. Aubert, "Aging and nonlinear heart rate control in a healthy population," Am. J. Physiol. Heart. Circ. Physiol. 290, H2560–H2570 (2006).

[41] A. L. Goldberger, C. K. Peng, and L. A. Lipsitz, "What is physiologic complexity and how does it change with aging and disease?," Neurobiol. Aging 23, 23–26 (2002).

[42] A. Voss, S. Schulz, R. Schroeder, M. Baumert, and P. Caminal, "Methods derived from nonlinear dynamics for analysing heart rate variability," Phil. Trans. R. Soc. A 367, 277–296 (2009).

[43] H. Wu, P. Hsu, C. Lin, H. Wang, C. Sun, A. Liu, et al, "Multiscale entropy analysis of pulse wave velocity for assessing atherosclerosis in the aged and diabetic," IEEE Trans. Biomed. Eng. 58, 2978–2981 (2011).

[44] D. E. Vaillancourt and K. M. Newell, "Changing complexity in human behavior and physiology through aging and disease," Neurobiol. Aging 23, 1–11 (2002).

[45] D. T. Kaplan, M. I. Furman, S. M. Pincus, S. M. Ryan, L. A. Lipsitz, and A. L. Goldberger, "Aging and the complexity of cardiovascular dynamics," Biophys. J. 59, 945 (1991).

[46] D. R. Seals and M. D. Esler, "Human ageing and the sympathoadrenal system," J. Physiol. 528, 407–417 (2000).

[47] E. G. Lakatta, "Cardiovascular regulatory mechanisms in advanced age," Physiol. Rev. 73, 413–467 (1993).

[48] H. Wu, C. Liu, M. Lo, P. Hsu, A. Liu, K. Chang, and C. Tang, "Multiscale cross-approximate

entropy analysis as a measure of complexity among the aged and diabetic," Comput. Math. Methods Med. 2013, (2013).

[49] B. Manor and L. A. Lipsitz, "Physiologic complexity and aging: Implications for physical function and rehabilitation," Prog. Neuropsychopharmacol. Biol. Psychiatry 45, 287–293 (2013).

[50] M. Kyriazis, "Practical applications of chaos theory to the modulation of human ageing: nature prefers chaos to regularity," Biogerontology 4, 75–90 (2003).

[51] L. A. Lipsitz and A. L. Goldberger, "Loss of 'complexity' and aging: potential applications of fractals and chaos theory to senescence," JAMA 267, 1806–1809 (1992).

[52] M. Baumert, B. Czippelova, A. Porta, and M. Javorka, "Decoupling of QT interval variability from heart rate variability with ageing," Physiol. Meas. 34, 1435 (2013).

[53] I. V. Tikhonova, A. V. Tankanag, and N. K. Chemeris, "Time–amplitude analysis of skin blood flow oscillations during the post-occlusive reactive hyperemia in human," Skin Res. Technol. 19, e174–e181 (2013).

[54] G. B. Yvonne-Tee, A. H. Rasool, A. S. Halim, A. R. Wong, and A. R. Rahman, "Method optimization on the use of postocclusive hyperemia model to assess microvascular function," Clin. Hemorheol. Microcirc. 38, 119–133 (2008).

[55] N. R. Harris and R. E. Rumbaut, "Age-related responses of the microcirculation to ischemia-reperfusion and inflammation," Pathophysiology 8, 1–10 (2001).

[56] E. Konstantinova, T. Tolstaya, S. Prishchep, A. Milutin, E. Mironova, and L. Ivanova, "Plasma lipid levels, blood rheology, platelet aggregation, microcirculation state and oxygen transfer to tissues in young and middle-aged healthy people," Clin. Hemorheol. Microcirc. 30, 443–448 (2004).

[57] R. Ogrin, P. Darzins, and Z. Khalil, "Age-related changes in microvascular blood flow and transcutaneous oxygen tension under basal and stimulated conditions," J. Gerontol. Ser. A-Biol. Sci. Med. Sci. 60, 200–206 (2005).

[58] T. Ryan, "The ageing of the blood supply and the lymphatic drainage of the skin," Micron. 35, 161–171 (2004).

[59] R. I. Kelly, R. Pearse, R. H. Bull, J. L. Leveque, J. de Rigal, and P. S. Mortimer, "The effects of aging on the cutaneous microvasculature," J. Am. Acad. Dermatol. 33, 749–756 (1995).

[60] J. P. Noon, B. R. Walker, D. J. Webb, A. C. Shore, D. W. Holton, H. V. Edwards, and G. C. Watt, "Impaired microvascular dilatation and capillary rarefaction in young adults with a

predisposition to high blood pressure," J. Clin. Invest. 99, 1873 (1997).

[61] E. Sadoun and M. Y. Reed, "Impaired angiogenesis in aging is associated with alterations in vessel density, matrix composition, inflammatory response, and growth factor expression," J. Histochem. Cytochem. 51, 1119–1130 (2003).

[62] P. E. Gates, W. D. Strain, and A. C. Shore, "Human endothelial function and microvascular ageing," Exp. Physiol. 94, 311–316 (2009).

[63] F. Bari, V. Tóth-Szűki, F. Domoki, and J. Kálmán, "Flow motion pattern differences in the forehead and forearm skin: age-dependent alterations are not specific for alzheimer's disease," Microvasc. Res. 70, 121–128 (2005).

[64] W. L. Kenney and T. A. Munce, "Invited review: aging and human temperature regulation," J. Appl. Physiol. 95, 2598–2603 (2003).

[65] M. El-Domyati, S. Attia, F. Saleh, D. Brown, D. E. Birk, F. Gasparro, H. Ahmad, and J. Uitto, "Intrinsic aging vs. photoaging: a comparative histopathological, immunohistochemical, and ultrastructural study of skin," Exp. Dermatol. 11, 398–405 (2002).

[66] B. A. Gilchrest, "Skin aging and photoaging: an overview," J. Am. Acad. Dermatol. 21, 610–613 (1989).

[67] J. M. Waller, and H. I. Maibach, "Age and skin structure and function, a quantitative approach (I): blood flow, pH, thickness, and ultrasound echogenicity," Skin Res. Technol. 11, 221–235 (2005).

[68] M. T. Lo, Y. C. Chang, C. Lin, H. W. Young, Y. H. Lin, Y. L. Ho, C. K. Peng, K. Hu, "Outlier-resilient complexity analysis of heartbeat dynamics," Sci. Rep. 5, 1–7 (2015).

[69] T. Söderström, A. Stefanovska, M. Veber, and H. Svensson, "Involvement of sympathetic nerve activity in skin blood flow oscillations in humans," Am. J. Physiol, Heart Circ. Physiol. 284, H1638–H1646 (2003).

[70] H. Kvernmo, A. Stefanovska, K. A. Kirkebøen, and K. Kvernebo, "Oscillations in the human cutaneous blood perfusion signal modified by endothelium-dependent and endothelium-independent vasodilators," Microvasc. Res. 57, 298–309 (1999).